Chiral Templating Activity of Tris(bipyridine)ruthenium(II) Cation in the Design of Three-Dimensional (3D) Optically Active Oxalate-Bridged $\{[Ru(bpy)_3][Cu_{2x}Ni_{2(1-x)}(C_2O_4)_3]\}_n$ ($0 \leq x \leq 1$; bpy = 2,2′-bipyridine): Structural, Optical, and Magnetic Studies

Fabrice Pointillart,[†] Cyrille Train,*[,†] Michel Gruselle,[†] Françoise Villain,[†,‡] Helmut W. Schmalle,[§] Delphine Talbot,[∥] Patrick Gredin,[⊥] Silvio Decurtins,[#] and Michel Verdaguer[†]

Laboratoire de Chimie Inorganique et Matériaux Moléculaires, Unité CNRS 7071, Université Pierre et Marie Curie (UPMC), 4 place Jussieu, Case 42, 75252 Paris Cedex 05, France, LURE, Bât. 209D, Université Paris-Sud, BP34, 91898 Orsay Cedex, France, Anorganisch Chemisches Institut, Universität Zürich, Winterthurerstrasse 190, CH-8057 Zürich, Switzerland, Liquides Ioniques et Interfaces Chargées, Unité CNRS 7612, UPMC, 4 place Jussieu, Case 63, 75252 Paris Cedex 05, France, Laboratoire de Cristallochimie du Solide, UPMC, 4 place Jussieu, Case 176, 75252 Paris Cedex 05, France, and Departement für Chemie und Biochemie, Universität Bern, Freiestrasse 3, CH-3012 Bern, Switzerland

Received December 30, 2002. Revised Manuscript Received August 21, 2003

Three-dimensional oxalate-based $\{[Ru(bpy)_3][Cu_{2x}Ni_{2(1-x)}(ox)_3]\}_n$ ($0 \leq x \leq 1$, ox = $C_2O_4^{2-}$, bpy = 2,2′bipyridine) were synthesized. The structure was determined for $x = 1$ by X-ray diffraction on single crystal. The compound crystallizes in the cubic space group $P4_132$. It shows a three-dimensional 10-gon 3-connected (10,3) anionic network where copper(II) has an unusual tris(bischelated) environment. X-ray powder diffraction patterns and their Rietveld refinement show that all the compounds along the series are isostructural and single-phased. According to X-ray absorption spectroscopy, copper(II) and nickel(II) have an octahedral environment, respectively elongated and trigonally distorted. As shown by natural circular dichroism, the optically active forms of $\{[Ru(bpy)_3][Cu_xNi_{2(1-x)}(ox)_3]\}_n$ are obtained starting from resolved Δ- or Λ-$[Ru(bpy)_3]^{2+}$. The Curie−Weiss temperatures range between −55 ($x = 1$) and −150 K ($x = 0$). The antiferromagnetic exchange interaction thus decreases when the copper contents increases in agreement with the crystallographic structure of the compounds and the electronic structure of the metal ions. At low temperature, the compounds exhibit complex long-range ordered magnetic behavior.

Introduction

Synthesizing materials combining magnetism with another physical property is one of the major present trends in molecular magnetism. An interesting challenge in this field is the obtention of chiral magnets,[1−24] presenting at the same time magnetic circular dichroism (Faraday effect), natural circular dichroism (Cotton

* To whom correspondence should be addressed. E-mail: train@ccr.jussieu.fr.
[†] Laboratoire de Chimie Inorganique et Matériaux Moléculaires, Unité CNRS 7071, UPMC.
[‡] Université Paris-Sud.
[§] Universität Zürich.
[∥] Liquides Ioniques et Interfaces Chargées, Unité CNRS 7612, UPMC.
[⊥] Laboratoire de Cristallochimie du Solide, UPMC.
[#] Universität Bern.

(1) Caneschi, A.; Gatteschi, D.; Rey, P.; Sessoli, R. *Inorg. Chem.* **1991**, *30*, 3936.
(2) Kumagai, H.; Inoue, K. *Angew. Chem., Int. Ed. Engl.* **1999**, *38*, 1601.
(3) Inoue, K.; Imai, H.; Ghalsasi, P. S.; Kikuchi, K.; Ohba, M.; Okawa, H.; Yakhmi, J. V. *Angew. Chem., Int. Ed.* **2001**, *40*, 4242.
(4) Inoue, K.; Kikuchi, K.; Ohba, M.; Okawa, H. *Angew. Chem., Int. Ed.* **2003**, *42*, 4810.
(5) Coronado, E.; Gomez-Garcia, C. J.; Nuez, A.; Romero, F. M.; Rusanov, E.; Stoeckli-Evans, H. *Inorg. Chem.* **2002**, *41*, 4615.
(6) Coronado, E.; Gimenez-Saiz, C.; Martinez-Agudo, J. M.; Nuez, A.; Romero, F. M.; Stoeckli-Evans, H. *Polyhedron* **2003**, *22*, 2435.
(7) Minguet, M.; Luneau, D.; Lhotel, E.; Villar, V.; Paulsen, C.; Amabilino, D. B.; Veciana, J. *Angew. Chem., Int. Ed.* **2002**, *41*, 586.
(8) Minguet, M.; Luneau, D.; Paulsen, C.; Lhotel, E.; Gorski, A.; Waluk, J.; Amabilino, D. B.; Veciana, J. *Polyhedron* **2003**, *22*, 2349.
(9) Decurtins, S.; Schmalle, H. W.; Schneuwly, P.; Oswald, H. R. *Inorg. Chem.* **1993**, *32*, 1888.
(10) Decurtins, S.; Schmalle, H. W.; Schneuwly, P.; Ensling, J.; Guetlich, P. *J. Am. Chem. Soc.* **1994**, *116*, 9521.
(11) Decurtins, S.; Schmalle, H. W.; Pellaux, R.; Schneuwly, P.; Hauser, A. *Inorg. Chem.* **1996**, *35*, 1451.
(12) Hernandez-Molina, M.; Lloret, F.; Ruiz-Perez, C.; Julve, M. *Inorg. Chem.* **1998**, *37*, 4131.
(13) Sieber, R.; Decurtins, S.; Stoeckli-Evans, H.; Wilson, C.; Yufit, D.; Howard, J. A. K.; Capelli, S. C.; Hauser, A. *Chem. Eur. J.* **2000**, *6*, 361.
(14) Coronado, E.; Galan-Mascaros, J. R.; Gomez-Garcia, C. J.; Martinez-Agudo, J. M. *Inorg. Chem.* **2001**, *40*, 113.
(15) Andres, R.; Brissard, M.; Gruselle, M.; Train, C.; Vaissermann, J.; Malezieux, B.; Jamet, J.-P.; Verdaguer, M. *Inorg. Chem.* **2001**, *40*, 4633.
(16) Tamaki, H.; Zhong, Z. J.; Matsumoto, N.; Kida, S.; Koikawa, M.; Achiwa, N.; Hashimoto, Y.; Okawa, H. *J. Am. Chem. Soc.* **1992**, *114*, 6974.

10.1021/cm020330d CCC: $27.50
Published on Web 02/13/2004

effect), and therefore possible cross-effects.[25,26] Different synthetic strategies were recently designed and developed to introduce chirality in the network through either chiral ligands (including radicals)[2−8] or the helicoidal chirality of the metallic center.[7,8,14,15,23] Among them, studies on oxalate-based networks have shown that these compounds are good candidates to design two- and three-dimensional multifunctional magnets[9−24] and are promising systems[14,15,23] for the study of cross-effects such as magneto-chiral dichroism.[25,26]

From a structural point of view, oxalate-based magnets are known as 3D[9−15] or 2D[16−23] networks. In the latter case, the 2D honeycomb anionic network can accommodate numerous types of cations to compensate its charge. This versatility has been widely exploited to introduce a new physical function, through the countercation.[17,21−24] The variety of shape and size of the countercations shows that there is not any strong size or symmetry requirements for this moiety. In contrast, in 3D compounds, the relationship between the cation and the three-dimensional 10-gon 3-connected (10,3) anionic network is much tighter. From a topological point of view, it has been clearly shown that the cation must be of appropriate symmetry (D_3), charge, and size.[9,10,14,15] The close link between the anionic and the cationic networks has been beautifully evidenced by the luminescence from the ^2E state of $[Cr(bpy)_3]^{3+}$ resulting from the absorption of a photon by $[Cr(ox)_3]^{3-}$ in $\{[Cr(bpy)_3][ClO_4][NaCr(ox)_3]\}_n$ and by the thermal spin transition observed in $\{[Co(bpy)_3][LiCr(ox)_3]\}_n$.[11,13] From a chemical point of view, Decurtins et al. synthesized 3D $\{[M^{II}(bpy)_3][\mathbf{M}^{II}_2(ox)_3]\}_n$ (M = Fe, Ni; **M** = Mn, Fe, Co, Zn) starting from *rac*-$[M^{II}(bpy)_3]^{2+}$, a $\mathbf{M}^{II}$ salt, and oxalic acid as precursors.[9] This result emphasizes the ability of these D_3 cations to template the self-assembling of an anionic network with the desired topology. Moreover, starting from racemic tris(oxalato)chromate(III) building blocks and optically active ruthenium cations, Andrés et al. showed that the ruthenium cations play a chiral template effect leading to optically active 3D compounds.[15]

In tris(oxalato)chromate-(III) and tris(oxalato)ferrate-(III)-based magnets, long-range magnetic ordering appears between 5.3 and 44 K.[14−16,18,23] To exploit more easily the multifunctionality of these compounds, it would be important to enhance their critical temperature. Modifying the metal ions bridged by the ligand in a rational way has been shown to be a powerful pathway toward high-temperature molecule-based magnets.[27,28] The oxalate bridge can transmit efficiently the interaction between two copper atoms: the antiferromagnetic exchange interaction can be as high as $-380\ cm^{-1}$.[29] But a $\{[A][Cu^{II}Cu^{II}(ox)_3]\}_n$ network would be an antiferromagnet. To take advantage of this strong antiferromagnetic exchange interaction and to obtain a nonzero resulting magnetization, we decided to study $\{[A][Cu_{2x}^{II}Ni^{II}_{2(1-x)}(ox)_3]\}_n$ networks because Cu^{II} ($S = 1/2$) and Ni^{II} ($S = 1$) ions bear different spins. We report hereafter the synthesis of selected $\{[Ru(bpy)_3][Cu_{2x}^{II}Ni^{II}_{2(1-x)}(ox)_3]\}_n$ compounds noted $\{Cu_{2x}Ni_{2(1-x)}\}_n$ ($0 \le x \le 1$), together with their structural, optical, and preliminary magnetic properties.

Experimental Section

Materials. $[Ru(bpy)_3]X_2$ (X = Cl, I, ClO_4) compounds were prepared according to literature methods.[30] Already described procedures of resolution have been followed to obtain enantiomerically pure or enriched Δ- and Λ-isomers of $[Ru(bpy)_3]^{2+}$.[31] The other reagents are commercially available and were used as purchased.

Synthesis of *rac*-$\{[Ru(bpy)_3][Cu_{2x}Ni_{2(1-x)}(ox)_3]\}_n$. The methodology to synthesize all the compounds in high yield and high purity is illustrated by the procedure used to obtain the racemic form of $\{Cu_{1.28}Ni_{0.72}\}_n$ ($x = 0.64$). Yields, IR, and elemental analysis are given below. Experimental values of C, H, and N come from elemental analysis. Experimental Ni and Cu values come from atomic absorption spectroscopy and correspond to the Cu-to-Ni ratio appearing in Table 3.

$\{[Ru(bpy)_3][Cu_{2x}Ni_{2(1-x)}(ox)_3]\}_n$ ($x = 0.64$). An aqueous solution (15 cm^3) containing 39.4 mg of $H_2C_2O_4{\cdot}2H_2O$ (0.31 mmol) is slowly added with stirring to an aqueous solution (10 cm^3) containing 77.9 mg of $[Ru(bpy)_3]Cl_2$ (0.1 mmol), 25.4 mg of $Cu(NO_3)_2{\cdot}3H_2O$ (0.1 mmol), and 30.5 mg of $Ni(NO_3)_2{\cdot}6H_2O$ (0.1 mmol). An orange precipitate starts to appear after a few minutes. After 15 min, the precipitate is filtered off, washed with water, and air-dried to yield 70.7 mg (71%) of an orange solid characterized as $\{[Ru(bpy)_3][Cu_{1.28}Ni_{0.72}(ox)_3]\}_n$. IR (KBr) cm^{-1}: 3083, m; 1627, s; 1589, vs; 1458, m; 1421, m; 1359, w; 1308, m; 1268, m; 800, m; 777, s; 490, m; 410, w. Anal. Calcd for $C_{36}H_{24}N_6O_{12}Cu_{1.28}Ni_{0.72}Ru$: C, 45.24; H, 2.53; N, 8.79. Found: C, 44.20; H, 2.68; N, 8.85; Cu, 8.50; Ni, 4.60.

$\{[Ru(bpy)_3][Cu_2(ox)_3]\}_n$. Yield: 86.7%. IR (KBr) cm^{-1}: 3082, m; 1635, s; 1586, vs; 1458, m; 1420, m; 1357, w; 1305, m; 1267, m; 802, m; 777, s; 491, m; 408, w. Anal. Calcd for $C_{36}H_{24}N_6O_{12}Cu_2Ru$: C, 45.00; H, 2.52; N, 8.75. Found: C, 44.09; H, 2.62; N, 8.80.

$\{[Ru(bpy)_3][Cu_{1.8}Ni_{0.2}(ox)_3]\}_n$. Yield: 78.3%. IR (KBr) cm^{-1}: 3082, m; 1631, s; 1586, vs; 1459, m; 1421, m; 1358, w; 1307, m; 1268, m; 801, m; 777, s; 490, m; 407, w. Anal. Calcd for $C_{36}H_{24}N_6O_{12}Cu_{1.5}Ni_{0.5}Ru$: C, 45.12; H, 2.52; N, 8.77. Found: C, 44.61; H, 2.76; N, 8.82; Cu, 11.98; Ni, 1.16.

$\{[Ru(bpy)_3][Cu_{0.88}Ni_{1.12}(ox)_3]\}_n$. The precipitate is filtered after 45 min. Yield: 73.4%. IR (KBr) cm^{-1}: 3084, m; 1627, s; 1592, vs; 1458, m; 1421, m; 1361, w; 1309, m; 1268, m; 799, m; 777, s; 491, m; 408, w. Anal. Calcd for $C_{36}H_{24}N_6O_{12}Cu_{0.5}Ni_{1.5}Ru$: C, 45.35; H, 2.54; N, 8.81. Found: C, 44.49; H, 2.83; N, 9.03; Cu, 5.92; Ni, 6.82.

(17) Kurmoo, M.; Graham, A. W.; Day, P.; Coles, S. J.; Hursthouse, M. B.; Caulfield, J. L.; Singleton, J.; Pratt, F. L.; Hayes, W.; Ducasse, L.; Guionneau, P. *J. Am. Chem. Soc.* **1995**, *117*, 12209.
(18) Mathoniere, C.; Nuttall, C. J.; Carling, S. G.; Day, P. *Inorg. Chem.* **1996**, *35*, 1201.
(19) Zhilyaeva, E. I.; Bogdanova, O. A.; Lyubovskaya, R. N.; Ovanesyan, N. S.; Pirumova, S. I.; Roshchupkina, O. S. *Synth. Met.* **1997**, *85*, 1663.
(20) Pellaux, R.; Schmalle, H. W.; Huber, R.; Fischer, P.; Hauss, T.; Ouladdiaf, B.; Decurtins, S. *Inorg. Chem.* **1997**, *36*, 2301.
(21) Coronado, E.; Galan-Mascaros, J. R.; Gomez-Garcia, C. J.; Laukhin, V. *Nature (London)* **2000**, *408*, 447.
(22) Lacroix, P. G. *Chem. Mater.* **2001**, *13*, 3495.
(23) Malezieux, B.; Andres, R.; Brissard, M.; Gruselle, M.; Train, C.; Herson, P.; Troitskaya, L. L.; Sokolov, V. I.; Ovseenko, S. T.; Demeschik, T. V.; Ovanesyan, N. S.; Mamed'yarova, I. A. *J. Organomet. Chem.* **2001**, *637−639*, 182.
(24) Clement, R.; Decurtins, S.; Gruselle, M.; Train, C. *Monatsh. Chem.* **2003**, *134*, 117.
(25) Rikken, G. L. J. A.; Raupach, E. *Nature (London)* **1997**, *390*, 493.
(26) Rikken, G. L. J. A.; Raupach, E. *Phys. Rev. E* **1998**, *58*, 5081.
(27) Ferlay, S.; Mallah, T.; Ouahes, R.; Veillet, P.; Verdaguer, M. *Nature (London)* **1995**, *378*, 701.
(28) Verdaguer, M.; Bleuzen, A.; Marvaud, V.; Vaissermann, J.; Seuleiman, M.; Desplanches, C.; Scuiller, A.; Train, C.; Garde, R.; Gelly, G.; Lomenech, C.; Rosenman, I.; Veillet, P.; Cartier, C.; Villain, F. *Coord. Chem. Rev.* **1999**, *190−192*, 1023.
(29) Alvarez, S.; Julve, M.; Verdaguer, M. *Inorg. Chem.* **1990**, *29*, 4500.
(30) Broomhead, J. A.; Young, C. G. *Inorg. Synth.* **1982**, *21*, 127.
(31) Dwyer, F. P.; Gyarfas, E. C. *J. Proc. R. Chem. Soc. N. S. W.* **1949**, *83*, 174.

$\{[Ru(bpy)_3][Cu_{0.3}Ni_{1.7}(ox)_3]\}_n$. The precipitate is filtered after 45 min. Yield: 79.5%. IR (KBr) cm^{-1}: 3084, m; 1625, s; 1593, vs; 1458, m; 1421, m; 1361, w; 1309, m; 1268, m; 798, m; 777, s; 491, m; 408, w. Anal. Calcd for $C_{36}H_{24}N_6O_{12}Cu_{0.2}Ni_{1.8}Ru$: C, 45.42; H, 2.54; N, 8.83. Found: C, 45.55; H, 2.63; N, 9.10; Cu, 2.00; Ni, 11.10.

$\{[Ru(bpy)_3][Ni_2(ox)_3]\}_n$. The precipitate is filtered after 45 min. Yield: 81.9%. IR (KBr) cm^{-1}: 3085, m; 1626, s; 1594, vs; 1458, m; 1421, m; 1361, m; 1309, s; 1268, m; 798, m; 777, s; 491, m; 408, w. Anal. Calcd for $C_{36}H_{24}N_6O_{12}Ni_2Ru$: C, 45.47; H, 2.54; N, 8.84. Found: C, 45.00; H, 2.89; N, 9.22.

Synthesis of Optically Active $\{[Ru(bpy)_3][Cu_{2x}Ni_{2(1-x)}(ox)_3]\}_n$. Two equivalents of $AgNO_3$ (107.1 mg, 0.63 mmol) is added to an aqueous solution (30 cm^3) containing 77.9 mg of resolved $[Ru(bpy)_3]I_2$ (233.6 mg, 0.315 mmol). The resulting AgI precipitate is filtered off. Then 76.1 mg of $Cu(NO_3)_2 \cdot 3H_2O$ (0.315 mmol) and 91.56 mg of $Ni(NO_3)_2 \cdot 6H_2O$ (0.315 mmol) are added to the filtrate. The aqueous solution of oxalic acid is slowly added with stirring to the resulting solution. An orange precipitate starts to appear after a few minutes. After 15 min, the precipitate is filtered off, washed with water, and air-dried.

$\{[\Delta Ru(bpy)_3][\Delta Cu_{1.28}\Delta Ni_{0.72}(ox)_3]\}_n$. The synthesis was made starting from $[\Delta Ru(bpy)_3]I_2$ (e.e. $= 0.9 \pm 0.1$). Yield: 197.4 mg (65.8%). IR (KBr) cm^{-1}: 3083, m; 1627, s; 1589, vs; 1458, m; 1421, m; 1359, w; 1308, m; 1267, m; 800, m; 777, s; 491, m; 408, w. Anal. Calcd for $C_{36}H_{24}N_6O_{12}CuNiRu$: C, 45.24; H, 2.53; N, 8.79. Found: C, 45.08; H, 2.71; N, 8.98.

$\{[\Lambda Ru(bpy)_3][\Lambda Cu_{1.28}\Lambda Ni_{0.72}(ox)_3]\}_n$. Synthesis was done starting from $[\Lambda Ru(bpy)_3]I_2$ (e.e. $= 1.0 \pm 0.1$).Yield: 208.0 mg (69.3%). IR (KBr) cm^{-1}: 3083, m; 1629, s; 1588, vs; 1458, m; 1421, m; 1359, w; 1308, m; 1267, m; 800, m; 777, s; 491, m; 408, w. Anal. Calcd for $C_{36}H_{24}N_6O_{12}CuNiRu$: C, 45.24; H, 2.53; N, 8.79. Found: C, 44.14; H, 2.63; N, 8.64.

Single-Crystal Growth. For growing single crystals,[32] a sodium metasilicate gel containing 0.01 mol L^{-1} oxalic acid was allowed to set in a test tube. Then, a stoichiometric quantity of a 0.01 mol L^{-1} aqueous solution of $[Ru(bpy)_3]Cl_2$ and copper(II) salt was added. Within several days, octahedral-shaped single crystals formed within the gel.

Physical Techniques. The IR spectra were recorded on a Bio-Rad IRFT spectrophotometer as KBr pellets in the 4000−250-cm^{-1} region. Elemental analyses were completed at the SIARE-UPMC, Paris. The nickel and copper concentrations were determined by atomic absorption spectrophotometry measurements using a Perkin-Elmer Analyst 100 apparatus. Specific rotations of the starting materials were measured at 20 °C, in a 1-dm tube containing the aqueous solution, using the sodium D line in a polarimeter Ameria AA5. The enantiomeric excesses were calculated by comparison with the maximum specific rotation values found in the literature. The results were confirmed by ^1H NMR spectroscopy using Δ-Trisphat (trisphat = tris(tetrachlorobenzene).[33] The spectra were recorded at room temperature in CD_2Cl_2 ($c = 1-2 \times 10^{-3}$ mol L^{-1}) in 5-mm tubes on a Bruker AC 300 spectrometer equipped with a QNP probehead. Natural circular dichroism spectra were recorded with a Jasco model J-710 spectropolarimeter. Measurements were made on 0.1−1 mg of solid dispersed in 100 mg of oven-dried KBr. Thirteen-millimeter diameter disks were made in a standard disk press. The displayed absorption spectra result from subtraction of the spectrum of a pure KBr disk followed by normalization at one of the dichroic signals for the extremum observed around 300 nm.

X-ray Crystallographic Analysis. Determination of unit cell parameters and collection of intensity diffraction data were performed at 183(2) K using an imaging plate detector system (Stoe IPDS diffractometer) with graphite-monochromated Mo Kα radiation. A total of 200 images were exposed at constant times of 1.50 min/image. The crystal-to-image distance was set to 48 mm ($\theta_{max} = 30.81°$). A ϕ rotation scan mode was selected for the ϕ increment of 1.0° per exposure. The total exposure time was 19 h. The intensities were integrated after using a dynamic peak profile analysis, and an estimated mosaic spread (EMS) check was used to prevent overlapping intensities.[34] A total of 8000 reflections with $I > 6\sigma(I)$ were selected out of the whole limiting sphere for the cell parameters refinement. Data reduction and numerical absorption correction[35] were performed using 16 indexed crystal faces; 44138 measured intensity data were merged to 1875 unique reflections, that is, 99.1% completeness of the data for $\theta_{max} = 30.81°$. Relevant crystallographic data and structure determination parameters for the cubic 3D structure of $\{Cu_2\}_n$ are given in Table 1. The observed systematic absences $h00$ with $h = 4n$ were in accordance with the possible space groups $P4_332$ or $P4_132$. The refinement was started with SHELXL-97[36] in space group $P4_332$ (No. 212) with coordinates taken from the known $\{Fe_2\}_n$ compound. [9] However, the absolute structure of the "delta"-form was clearly shown to be wrong with Flack's x-parameter of 0.99(3), and R-values were 4.24% and 10.36% for R1 and wR2, respectively. Thus, the space group choice was $P4_132$ (No. 213), indicating a Λ configuration for the tris-(bischelated) Ru and Cu centers.[37,38] The symmetry operators and the coordinates were inverted accordingly and the refinement converged rapidly with the correct absolute structure parameter $x = 0.01(2)$ and with the improved R-values given in Table 1. No twinning of merohedry was observed for the $\{Cu_2\}_n$ measured crystal. The positions of all H-atoms were calculated after each refinement cycle (riding model). The final maximum and minimum residual electron density values were 0.997 and −0.923 e/A^3. Graphic representation of Figure 1 has been created by using the program PLATON.[39]

The powder diffraction patterns were collected at room temperature on a Philips PW-1050 goniometer using the Bragg−Brentano configuration and Mn-filtered Fe Kα radiation. The X-ray powder patterns are first analyzed by the EVA program,[40,41] to verify the lack of the starting compounds and

Table 1. Crystal Data and Structure Refinement Characteristics for $\{Cu_2\}_n$

empirical formula	$C_{36}H_{24}Cu_2N_6O_{12}Ru$
formula weight	960.76
temperature	183(2) K
wavelength	0.71073 Å
crystal system, space group	cubic, $P4_132$ (No. 213)
unit cell dimensions	$a = b = c = 15.2966(7)$ Å $\alpha = \beta = \gamma = 90°$
volume	3579.2(3) $Å^3$
Z, calculated density	4, 1.783 Mg/m^3
absorption coefficient	1.669 mm^{-1}
$F(000)$	1920
crystal size	0.45 × 0.41 × 0.11 mm
theta range for data collection	2.98−30.81°
index ranges	$-11 \le h \le 12$, $0 \le k \le 15$, $2 \le l \le 21$
reflections collected/unique	44138/1875 [R(int) = 0.0529]
completeness to theta = 30.81	99.1%
absorption correction	numerical
max. and min. transmission	0.8377 and 0.5205
refinement method	full-matrix least-squares on F^2
data/restraints/parameters	1875/0/88
goodness-of-fit on F^2	0.920
final R indices [$I > 2\sigma(I)$]	R1 = 0.0272, wR2 = 0.0671
R indices (all data)	R1 = 0.0322, wR2 = 0.0683
absolute structure parameter	0.01(2)
largest diff. peak and hole	0.997 and −0.923 e $Å^{-3}$

(32) Henish, H. K. *Crystal growth in gel*; Pennsylvania State University: University Park, PA, 1973.
(33) Lacour, J.; Torche-Haldimann, S.; Jodry, J. J. *J. Chem. Soc., Chem. Commun.* **1998**, 1733.
(34) *Stoe IPDS software for data collection, cell refinement and data reduction*; 2.92; Stoe & Cie: Darmstadt, Germany, 1999.
(35) Coppens, P.; Leiserowitz, L.; Rabinovich, D. *Acta Crystallogr.* **1965**, *18*, 1035.
(36) Sheldrick, G. M. *SHELXL97*; University of Göttingen: Göttingen, Germany, 1997.
(37) Flack, H. D.; Bernardinelli, G. *Acta Crystallogr.* **1999**, *A55*, 908.
(38) Flack, H. D.; Bernardinelli, G. *J. Appl. Crystallogr.* **2000**, *33*, 1143.
(39) Spek, A. L. *Acta Crystallogr.* **1990**, *A46*, C34.

Table 2. Crystallographic Data and Structure Refinement Characteristics for $\{Ni_2\}_n$, $\{Cu_{0.88}Ni_{1.12}\}_n$, and $\{Cu_{1.8}Ni_{0.2}\}_n$

	$\{Ni_2\}_n$	$\{Cu_{0.88}Ni_{1.12}\}_n$	$\{Cu_{1.8}Ni_{0.2}\}_n$
crystal system, space group	cubic, $P4_132$ (No. 213)		
refined cell parameters			
a	15.2619(3) Å	15.2756(4) Å	15.3108(4) Å
volume	3554(3) Å^3	3564(3) Å^3	3589(3) Å^3
Z	4	4	4
X-ray radiation	Fe Kα_1 (1.93609 Å) and Fe Kα_2 (1.94003 Å)		
2θ data range and step	9−130° by 0.04°		
total counting time	3 s/step		
no. of independent reflections	381	372	372
no. of global parameters	4	5	5
no. of intensity-dependent parameters	30	30	30
half-width parameters			
$H^2 = U \tan^2\theta + V \tan\theta + W$			
U	0.21(1)	0.096(6)	0.058(5)
V	−0.09(1)	−0.067(4)	−0.037(4)
W	0.030(1)	0.0246(7)	0.0210(6)
η (pseudo-Voigt profile)	0.58(1)	0.55(1)	0.56(1)
asymmetry parameters:			
A_0	0.1036(2)	0.091(4)	0.093(4)
B_0	0.029(1)	0.0405(9)	0.0357(9)
Rietveld reliability factors (%)			
Rp	17.4	15.5	15.4
Rwp	19.8	17.5	17.6
Rexp	12.6	12.3	12.8
R_B	8.8	7.2	6.7
R_F	12.2	6.0	8.9
χ^2	2.5	2.0	1.9

the crystallinity of the material and to calculate *d*-spacings. The cell parameters are refined using the UFIT program.[42] Then the powder diffraction patterns for $\{Ni_2\}_n$,$\{Cu_{0.88}Ni_{1.12}\}_n$ and $\{Cu_{1.8}Ni_{0.2}\}_n$ were refined by the Rietveld method[43] using FULLPROF[44] starting from the atomic positions obtained by single-crystal X-ray diffraction of a single crystal of $\{[Ni(bpy)_3][Mn^{II}_2(ox)_3]\}_n$ in the $P4_132$ space group.[10] The refinement characteristics are reported in Table 2. The quality of the refinements is checked by using the values of the reliability factors and using the program PLOTR[45] by a careful graphical survey of the difference curve between the calculated and experimental patterns.

X-ray Absorption Spectroscopy (XAS). XAS experiments were performed on the XAS 13 beam line at the French synchrotron facility DCI at LURE (Orsay). Spectra were recorded at the copper and nickel K edges in transmission mode using Si 311 (XANES) and Si 111 (EXAFS) double monochromator. For the edge spectra, the spectra of the sample and the one of a copper or nickel foil were recorded simultaneously using a third ionization chamber to check energy calibration. The edge energies were fixed at the first inflection point of the metallic foils, 8979 eV for the copper and 8333 eV for the nickel. The samples were ground and homogeneously dispersed in cellulose pellets.

Edge spectra were recorded with 0.3 eV steps and an integration time equal to 1 s/point. The spectra were normalized at the middle of the first EXAFS oscillation. EXAFS spectra were recorded using 2 eV steps and an integration time equal to 2 s/point. The EXAFS signal treatment was performed with the "EXAFS pour le Mac" code.[46] The EXAFS signal was extracted from the data by subtracting a linear pre-edge background, a combination of polynomials and cubic spline atomic absorption background, and normalized by the Lengeler-Eisenberger procedure.[47] The pseudo-radial distribution function was given by the Fourier transform (FT) of $w(k)k^3\chi(k)$, where $w(k)$ is a Kaiser-Bessel window with a smoothness parameter equal to 3 (k is the wavenumber). The k limits are equal to 2.3−14 Å^{-1} (Δk = 11.7 Å^{-1}). The signals, calculated with the FEFF7 code,[48] of the first two shells of neighbors using the simple and multiple scattering schemes are the same. The experimental signal of the two first shells was thus simulated using the single scattering scheme with the Round Midnight program.[49] The amplitude ($|f_i(k,R_i)|$) and phase ($|\phi_i(k,R_i)|$ functions were calculated using the Mac Kale's amplitude and phase.[50]

Magnetic Measurements. The magnetization of powdered samples were measured between 2 and 300 K on a Quantum Design MPMS5 squid magnetometer. The hysteresis loops were measured at 2 K. The zero field cooled (ZFC), field cooled (FC), and remnant magnetization versus temperature were measured in a 0.01 T external field. The susceptibility was measured in a 0.1 T external field and corrected for diamagnetism and temperature-independent paramagnetism.

Results and Discussion

Synthesis. Synthesizing copper−nickel oxalate-based networks isostructural of those previously described in which the transition metal ions are in an octahedral environment is challenging since tris(oxalato)-cuprate(II) and -nickelate(II) complexes were never described. Anionic building blocks are thus lacking. Moreover, copper(II) and nickel(II) ions combined with oxalate organize as chains in which the metal ions are bonded to two oxalate ligands only.[51] To overcome these hindrances, we developed a synthetic strategy combining those described by Decurtins et al.[9] and Andrés et al.[15] It exploits the chiral template effect of the $[Ru(bpy)_3]^{2+}$

(40) Caussin, P.; Nusinovici, J.; Beard, D. W. *Adv. X-Ray Anal.* **1988**, *31*, 423.
(41) Caussin, P.; Nusinovici, J.; Beard, D. W. *Adv. X-Ray Anal.* **1989**, *32*, 531.
(42) Evain, M.; I. M. N.: Nantes, France, 1992.
(43) Rietveld, H. M. *J. Appl. Crystallogr.* **1969**, *2*, 65.
(44) Rodriguez-Carvajal, J. Satellite Meeting on Powder Diffraction of the XV Congress of the IUCr, Toulouse, France, 1990; p 127 (http://www-llb.cea.fr/fullweb/powder.htm).
(45) Roisnel, T. Laboratoire Léon Brillouin: CEA Saclay, France, 1995 (http://www-llb.cea.fr/fullweb/powder.htm).
(46) Michalowicz, A. *EXAFS pour le MAC*; Société Française de Chimie: Paris, France, 1991.
(47) Lengeler, B.; Eisenberger, P. *Phys. Rev. B* **1980**, *21*, 4507.
(48) Rehr, J. J.; Mustre de Leon, J.; Zabinsky, S. I.; Albers, R. C. *J. Am. Chem. Soc.* **1991**, *113*, 5135.
(49) James, F.; Roos, M. CERN Computing Center, Program Library, CERNID Internal Report 75/20, 1976.
(50) McKale, A. G.; Veal, B. W.; Paulikas, A. P.; Chan, S. K.; Knapp, G. S. *J. Am. Chem. Soc.* **1988**, *110*, 3763.
(51) Verdaguer, M.; Julve, M.; Michalowicz, A.; Kahn, O. *Inorg. Chem.* **1983**, *22*, 2624.

Table 3. Copper Fraction x : x_{sol}, Calculated Value in the Synthetic Solution, and x_{AAS}, Experimental Value in $\{Cu_{2x}Ni_{2(1-x)}\}_n$ Determined by Atomic Absorption Spectrophotometry (AAS)

x_{sol}	0.00	0.10	0.25	0.50	0.75	1.00
x_{AAS} in $\{Cu_{2x}Ni_{2(1-x)}\}_n$	0.00	0.15	0.44	0.64	0.90	1.00

cation to constrain copper and nickel ions to insert into a three-dimensional 10-gon 3-connected (10,3) oxalate-based network. The enantioselective reaction then writes for a Δ enantiomer:

$$n\ \Delta\text{-}[Ru(bpy)_3]^{2+} + 2nx\ Cu^{2+} + 2n(1-x)\ Ni^{2+} + 3n\ ox^{2-} \rightarrow \{[\Delta Ru(bpy)_3][\Delta Cu^{II}_{2x}\Delta Ni^{II}_{2(1-x)}(ox)_3]\}_n$$

To a solution containing the ruthenium(II) template cation mixed with nitrate salts of copper(II) and nickel(II), a solution of oxalic acid is added dropwise, leading to the slow formation of an orange precipitate. The precipitation becomes slower when the nickel-to-copper ratio increases. The procedure prevents the formation of chains since the metal ions react with oxalate only when the ruthenium cation is present.

The use of $[Ru(bpy)_3]^{2+}$ allows the control of the symmetry around the metal ions but does not bring any control on the relative insertion of nickel(II) and copper(II) ions in the 3D networks. The atomic absorption spectrophotometry measurements (Table 3) lead to the conclusion that the insertion in the network is easier for copper(II) than for nickel(II). This observation is supported by the increasing reaction time needed to obtain good yield when the nickel contents increase.

Structural Studies. According to single-crystal X-ray diffraction (XRD), the crystallographic structure of $\{Cu_2\}_n$ is very similar to the one of $\{[M(bpy)_3][\mathbf{M}(ox)_3]\}_n$ ($M = \mathbf{M} = Fe^{2+}$ and ($M = Ru^{2+}$ and $\mathbf{M} = Mn^{2+}$)):[9,10] the formal $[Cu(ox)_{3/2}]$ subunits, representing 3-connecting points, build up well-defined 10-gon 3-connected nets (10,3) with $[Ru(bpy)_3]^{2+}$ cations fitting the vacancies in strictly the same manner in the two compounds (Figure 1). Atomic numbering is shown in Figure 1 whereas Table 4 gathers selected bond lengths and angles. The $P4_132$ space group (Table 1) is a chiral cubic space group where all the tris(bischelated) metallic centers adopt the Λ configuration. A spontaneous resolution thus occurs during the crystallization. The oxalate bridge is symmetrical. The copper atom is located on the 3-fold axis. It is surrounded by three equivalent oxygen atoms O(11) located at 2.087(2) Å and three other equivalent oxygen atoms O(21) located at 2.109(2) Å. The O(11)−Cu(1)−O(21) angle is 79.28(7)° (Table 4). The environment of the copper(II) ion is thus described by XRD as a trigonally compressed octahedron.

Such a geometry is rare in the structural chemistry of copper(II) ion though it has already been observed by XRD in complexes such as $\{[Cu(en)_3]^{2+}, SO_4^{2-}\}$.[52] Nevertheless, in this case, EPR and X-ray absorption spectroscopy (XAS) demonstrated that due to Jahn−Teller effect, the environment of the Cu(II) ion, at room temperature, is indeed a dynamically distorted octahedron (four short and two long fluctuating distances). The relatively strong difference of the anisotropic displacement parameters for O(11) and O(21) (Table 5) is a strong indication that such a mechanism could be at work in $\{Cu_2\}_n$.[53−55] A closer look at the local geometry around copper in $\{Cu_2\}_n$ and, for comparison, around nickel in $\{Ni_2\}_n$ was undertaken by XAS to check this hypothesis.

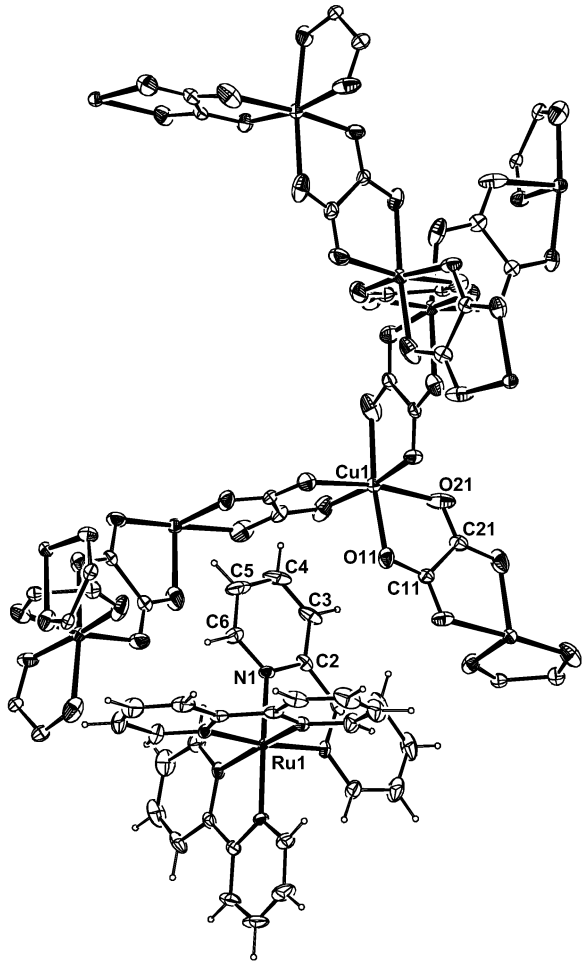

Figure 1. Ortep view[30] of a representative section of the 3D anionic network together with a $[Ru(bpy)_3]^{2+}$ template cation of the crystal structure of $\{Cu_2\}_n$. Displacement ellipsoids are shown at the 50% probability level.

Furthermore, since single crystals could not be obtained for stoichiometries different from $x = 1$, the structures were determined using X-ray powder diffraction. The patterns shown in Figure 2 for $\{Cu_{0.88}Ni_{1.12}\}_n$ ($x = 0.44$) are typical of those obtained for all the studied compounds. The diffractogram is composed of thin peaks, indicating a good crystallinity of the compounds. This is in accordance with the slow precipitation of the solid which allows good organization within the network. Figure 2 shows the results for $x = 0.44$ at the final stage of the refinement. The refined atomic positions for the three compounds $x = 0.00$, 0.44, 0.90 are the same within experimental errors and very close to those obtained by single-crystal XRD of $\{Cu_2\}_n$. Being able to perform the refinement without further hypothesis (metal ions ordering, multiphase system, etc.) indicates

(52) Villain, F.; Verdaguer, M.; Dromzee, Y. *J. Phys. IV* **1997**, *7*, 659.

(53) Hathaway, B. J.; Hodgson, P. G.; Power, P. C. *Inorg. Chem.* **1974**, *13*, 2009.

(54) Araya, M. A.; Cotton, F. A.; Daniels, L. M.; Falvello, L. R.; Murillo, C. A. *Inorg. Chem.* **1993**, *32*, 4853.

(55) Stebler, M.; Buergi, H. B. *J. Am. Chem. Soc.* **1987**, *109*, 1395.

Table 4. Selected Bond Lengths (Å) and Angles (deg) in the Coordination Sphere of the Metal Ions of the $\{Cu_{2x}Ni_{2(1-x)}\}_n$ Anionic Network, from Single-Crystal XRD ($x = 1$) and from Powder XRD[a]

Cu(1)−O(11)	2.087(2)
Cu(1)−O(21)	2.109(2)
O(11)−C(11)	1.250(2)
O(21)−C(21)	1.254(3)
C(11)−C(21)	1.551(5)
O(11)−Cu(1)−O(11)#4	90.98(8)
O(11)#5−Cu(1)−O(21)	91.81(8)
O(11)−Cu(1)−O(21)	79.38(7)
O(11)#4−Cu(1)−O(21)	170.01(8)
O(21)−Cu(1)−O(21)#4	98.13(7)
C(11)−O(11)−Cu(1)	113.56(18)
C(21)−O(21)−Cu(1)	113.20(19)
O(11)−C(11)−O(11)#6	125.4(3)
O(11)−C(11)−C(21)	117.29(17)
O(21)#6−C(21)−O(21)	127.5(4)
O(21)−C(21)−C(11)	116.24(18)
metal ions coordination sphere for $x \neq 1$	
Ni(1)−O(11)	2.03(2)[b]
Cu/Ni(1)−O(11)	2.05(2)[c]
Cu/Ni(1)−O(11)	2.02(2)[d]
Ni(1)−O(21)	2.15(2)[b]
Cu/Ni(1)−O(21)	2.11(1)[c]
Cu/Ni(1)−O(21)	2.15(1)[d]

[a] Symmetry transformations used to generate equivalent atoms: (#1) $-z + 7/4$, $-y + 7/4$, $-x + 7/4$; (#2) $-y + 7/4$, $-x + 7/4$, $-z + 7/4$; (#3) $-x + 7/4$, $-z + 7/4$, $-y + 7/4$; (#4) z, x, y; (#5) y, z, x; (#6) $z + 1/4$, $-y + 5/4$, $x - 1/4$. [b−d] Distances obtained from Rietveld refinement of powder diffraction data for [b]$\{Ni_2\}_n$, [c]$\{Cu_{0.88}Ni_{1.12}\}_n$, and [d]$\{Cu_{1.8}Ni_{0.2}\}_n$.

Table 5. Anisotropic Displacement Parameters (Å^2 × 10^3) for $\{Cu_2\}_n$; Anisotropic Displacement Factor Exponent Takes the Form $-2\pi^2[h^2A^{*2}U11 + ... + 2hkA^*b^*U12]$

	U11	U22	U33	U23	U13	U12
Ru(1)	9(1)	9(1)	9(1)	−1(1)	−1(1)	−1(1)
N(1)	15(1)	10(1)	22(1)	0(1)	0(1)	−1(1)
C(2)	10(1)	19(1)	23(1)	6(1)	1(1)	0(1)
C(3)	20(1)	19(1)	42(2)	16(1)	6(1)	2(1)
C(4)	32(2)	11(1)	65(2)	8(1)	9(1)	1(1)
C(5)	37(2)	15(1)	50(2)	−10(1)	2(1)	0(1)
C(6)	30(1)	17(1)	27(1)	−4(1)	−2(1)	−3(1)
Cu(1)	16(1)	16(1)	16(1)	−1(1)	−1(1)	−1(1)
O(11)	14(1)	27(1)	36(1)	4(1)	2(1)	1(1)
O(21)	53(1)	41(1)	16(1)	0(1)	−4(1)	−17(1)
C(11)	18(1)	13(1)	18(1)	3(1)	2(1)	−3(1)
C(21)	21(1)	20(2)	21(1)	5(1)	0(1)	−5(1)

the existence of solid solutions all along the series. Then, all compounds are isomorphous, for example, 3D (10,3) anionic networks wrapped around the ruthenium(II) template cation. The cell parameter of the compounds increases monotonically from 15.2619(3) Å for $x = 0$ to 15.3212(16) Å for $x = 1$ (Table 2). The evolution is close to what is expected from the Vegard's law in accordance with the formation of single-phased solid solutions with a statistical distribution of the Ni(II) and Cu(II) ions on the metal sites of the anionic network.

XAS measurements at the copper K edge for $\{Cu_2\}_n$ and at the nickel K edge for $\{Ni_2\}_n$ bring complementary information about the local geometry around the metal ion. Figure 3 shows the edge spectra of $\{Cu_2\}_n$ and $\{Ni_2\}_n$ together with the spectra of reference compounds, for example, ($\{[Cu(en)_2]^{2+}, 2NO_3^-\}$, $\{[Cu(en)_3]^{2+}, SO_4^{2-}\}$, $[Cu(H_2O)_6]^{2+}$ for Cu(II) and $[Ni(H_2O)_6]^{2+}$ for Ni(II).[52,56]

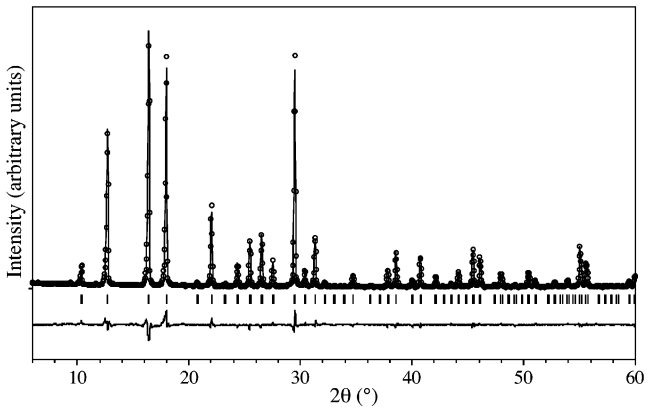

Figure 2. Observed (circle) and calculated (full curve) X-ray powder pattern diffraction profile of $\{Cu_{0.88}Ni_{1.12}\}_n$ at room temperature. The short vertical lines below the profile curves mark all possible Bragg reflections. The lower curve shows the difference between observed and calculated profiles.

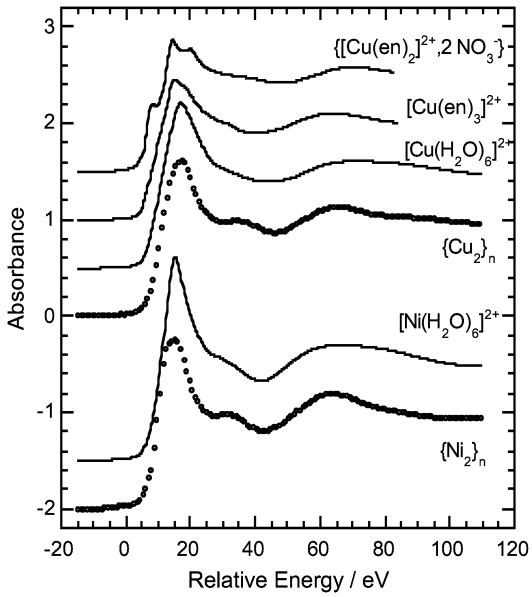

Figure 3. XANES signal at copper K-edge for $[Cu(en)_2]^{2+}$, $[Cu(en)_3]^{2+}$, $[Cu(H_2O)_6]^{2+}$, and $\{Cu_2\}_n$ and at nickel K-edge for $[Ni(H_2O)_6]^{2+}$ and $\{Ni_2\}_n$.

In $\{[Cu(en)_2]^{2+}, 2NO_3^-\}$, the Cu(II) ion adopts a quasi square planar geometry (4 N at 2.02 Å and two oxygen atoms at very long distances, e.g., 2.60 Å) which splits the degeneracy of the vacant 4p orbitals into two sets: p_z is left unchanged at low energy and $p_{x,y}$ are pushed at high energy by an antibonding interaction with the ligands. Accordingly the edge spectrum shows an intense peak in the rising edge region (8987.1 eV) (allowed $1s \rightarrow p_z$ transition) followed at higher energy (8993.5 eV) by the allowed $1s \rightarrow p_{x,y}$ transition. In $\{[Cu(en)_3]^{2+}, SO_4^{2-}\}$ and $[Cu(H_2O)_6]^{2+}$, due to Jahn−Teller effect, the environment of the Cu(II) ion is a dynamically distorted octahedron: four short and two long fluctuating distances (4 + 2).[52] The similarity of the spectra of the last two compounds and the one of $\{Cu_2\}_n$ confirms the 4 + 2 distorted octahedral geometry around the Cu(II) ion rather than a square planar one. The edge of $[Ni(H_2O)_6]^{2+}$ consists of a sharp "white line" assigned to an allowed $1s \rightarrow 4p_{x,y,z}$ transition; the 4p orbitals are degenerate according to the regular octahedral geometry of the complex. The edge of $\{Ni_2\}_n$ is smoother and the transitions are wider when compared to the ones of

(56) Briois, V.; Lagarde, P.; Brouder, C.; Sainctavit, P.; Verdaguer, M. *Physica B (Amsterdam)* **1995**, *208−209*, 51.

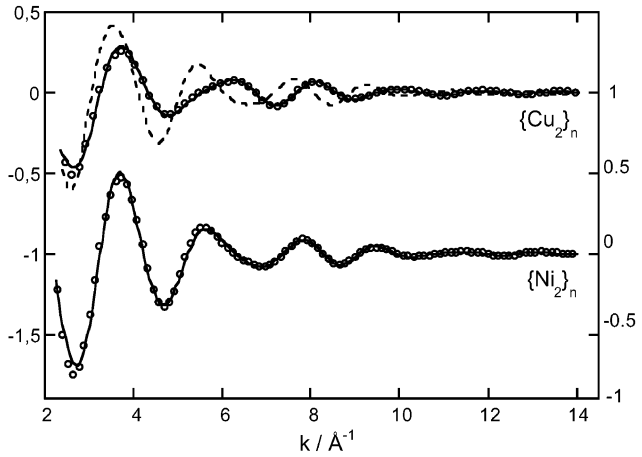

Figure 4. Experimental EXAFS signal at K-edge of $\{Cu_2\}_n$ and $\{Ni_2\}_n$ arising from the first two shells (open circles) compared to the simulation using the optimized geometry described in Table 6 (solid line) and, for $\{Cu_2\}_n$, the data deduced from X-ray diffraction (dotted line).

hexaaquanickel(II) as expected from the energy distribution of the Ni(II) ion 4p orbitals due to the trigonal distortion of the octahedron as observed by X-ray powder diffraction (Table 2). Two further pieces of information arise from the edge spectra of $\{Cu_2\}_n$ and $\{Ni_2\}_n$: (i) the weak intensities in the pre-edge region confirm the presence of a very symmetric site at Cu and Ni (1s to 3d forbidden transitions); (ii) the feature clearly observed at 30 eV above the edge, in the two oxalate compounds only, corresponds to multiple scattering effects due to OCM angle close to 180° usually observed in oxalate-chelated complexes (Scheme 1).[51]

Scheme 1

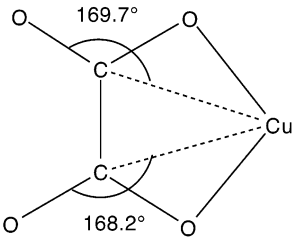

The above qualitative description of the local geometry can be completed by the EXAFS quantitative analysis. FEFF[48,57] calculations were performed using the XRD atomic coordinates of $\{Cu_2\}_n$ in the single or the multiple scattering frame. It follows that multiple scattering (i) strongly influences the signal of the third shell of neighbors (built from six oxygen atoms), due to the angles close to 170° for the Cu^{II}- -C−O scattering pathways (Scheme 1), in agreement with the features observed at 30 eV above the edge, and (ii) is negligible for the first two shells. So the analysis of the first two shells can be performed in the simple scattering approximation.

Figure 4 shows the comparison between the experimental and calculated signals of the first two shells for $\{Cu_2\}_n$ and $\{Ni_2\}_n$. For $\{Ni_2\}_n$ the geometry deduced from EXAFS measurements (Table 6) is in agreement with the powder XRD data (Table 2) within experimental errors. In contrast, the crystallographic data of $\{Cu_2\}_n$ do not fit properly the local order around the Cu(II) ion (Table 2). To account for the observed EXAFS signal, it is necessary to consider (i) an elongated geometry around the copper atom with four oxygen atoms located at 1.99 Å and two apical atoms at 2.32 Å and (ii) a large Debye−Waller factor for the two apical oxygen atoms (Table 6).

Table 6. Parameters Used in the EXAFS Simulation (Figure 4) for the Elongated Octahedral Environment of the Cu(II) in $\{Cu_2\}_n$ and for the Trigonally Distorted Geometry around the Ni(II) in $\{Ni_2\}_n$.

central atom	neighbors	N	R/Å	σ/Å	Γ	ΔE_0/eV
Cu	O_1	4	1.99	0.07	1.0	0.5
Cu	O_2	2	2.33	0.13	1.0	0.5
Cu	C	6	2.77	0.10	1.0	−8.2
Ni	O_1	3	2.04	0.05	0.7	5
Ni	O_2	3	2.14	0.05	0.7	5
Ni	C	6	2.80	0.07	0.7	0

The oxalate coordination to copper observed in $\{Cu_2\}_n$ is not common for μ-oxalato-bridged copper(II) complexes. Indeed, the geometry around the copper atom is usually nearly square planar or square pyramidal.[29,51,58−60] In μ-oxalato copper(II)−nickel(II) ribbon chains, the copper atom happens to be surrounded by six oxygen atoms. Four are coming from two oxalate equatorial ligands while the two others are belonging to two oxalates of neighboring chains.[51] Nevertheless, copper atom surrounded by three coordinated oxalate groups is known in 2D oxalate-based magnets[16] and in a 1D helical chain[61] obtained by oxidation of a mixture of copper(II), vitamin C, and 2-diethylaminoethanol in the presence of H_2O_2. In the former case, no single-crystal diffraction data are available. In the later case, the X-ray diffraction reveals a *compressed* octahedral environment around the copper atom, for example, two short Cu−O distances (1.99−2.00Å) and four long Cu−O distances (2.09−2.15 Å). Such a compressed geometry of the copper(II) is also observed in the XRD structure of $\{[Cu(en)_3]^{2+}, SO_4^{2-}\}$ at low temperature, while at room temperature the CuN_6 octahedron appears regular.[52] XAS studies on this complex revealed that at both temperatures the local geometry around the copper atom is an elongated octahedron (4 + 2 geometry). The authors assign this apparent difference between XRD and XAS to dynamic Jahn−Teller effect at room temperature and static Jahn−Teller effect combined with an antiferrodistortive order at low temperature. This study reveals the complementarity of the two techniques (long and short range order), to fully describe the structure of systems where some disorder is present.[51,52]

The results obtained for $\{Cu_2\}_n$ by XRD and XAS are similar to the ones for $\{[Cu(en)_3]^{2+}, SO_4^{2-}\}$. The strong difference of the anisotropic displacement parameters of O(11) and O(21) (XRD, Table 5) and the large Debye−Waller factor of the apical oxygen atoms (EXAFS, Table 6) are consistent either with a dynamic Jahn−Teller effect on the copper centers or with a static Jahn−Teller

(57) Mustre de Leon, J.; Rehr, J. J.; Zabinsky, S. I.; Albers, R. C. *Phys. Rev. B* **1991**, *44*, 4146.

(58) Kahn, O. *Molecular Magnetism*; VCH: Weinhem, 1993.

(59) Julve, M.; Verdaguer, M.; Gleizes, A.; Philoche-Levisalles, M.; Kahn, O. *Inorg. Chem.* **1984**, *23*, 3808.

(60) Cano, J.; Alemany, P.; Alvarez, S.; Verdaguer, M.; Ruiz, E. *Chem. Eur. J.* **1998**, *4*, 476.

(61) Sundberg, M. R.; Kivekas, R.; Koskimies, J. K. *J. Chem. Soc., Chem. Commun.* **1991**, 526.

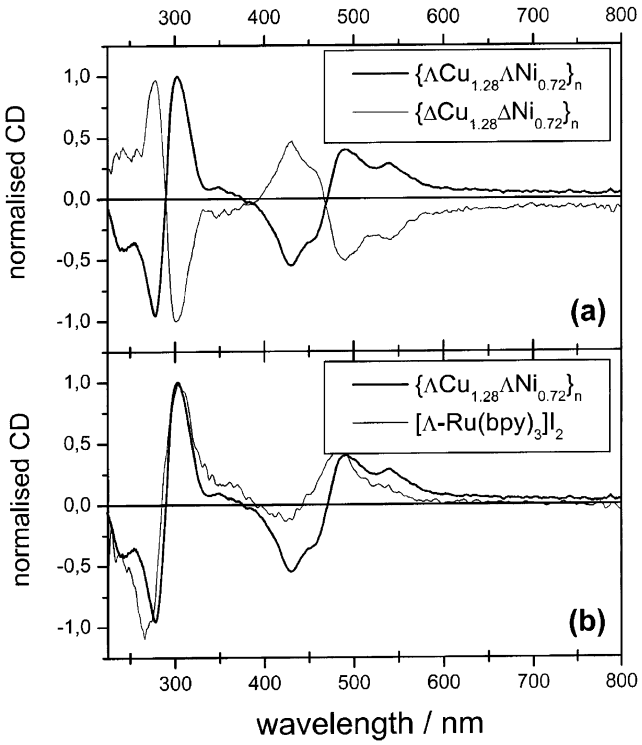

Figure 5. Natural circular dichroism spectra in KBr pellets of $\{\Delta Cu_{1.28}\Delta Ni_{0.72}\}_n$ and $\{\Lambda Cu_{1.28}\Lambda Ni_{0.72}\}_n$ (a) and $\{\Lambda Cu_{1.28}\Lambda Ni_{0.72}\}_n$ and $[\Lambda Ru(bpy)_3]I_2$ (b) in KBr pellets.

effect associated with a statistical distribution of the long Cu−O distances. It is rather difficult to decide which *scenario* is the most likely: on one hand, highly symmetrical space groups as in $\{Cu_2\}_n$ can be associated with a dynamic effect;[54,55] on the other hand, the important constraints existing in such 3D networks[11,13] make bond distances fluctuations as high as 0.3 Å unlikely. Nevertheless, the fact that the space group of the compound remains unchanged from room temperature down to 183 K is a second argument in favor of the presence of a statistically distributed static distortion in $\{Cu_2\}_n$.

Natural Circular Dichroism. Since the obtained polymers are insoluble, natural circular dichroism (NCD) was performed on solid-state samples. The NCD curves for $\{Cu_{1.28}Ni_{0.72}\}_n$ obtained with Δ- and Λ-$[Ru(bpy)_3]^{2+}$ are shown in Figure 5a. The two normalized spectra are opposite in sign, which asseses the enantioselective character of the reaction leading to the networks.

In Figure 5b, the NCD spectrum of $\{\Lambda Cu_{1.28}\Lambda Ni_{0.72}\}_n$ is compared to the one of the template cation salt Λ-$[Ru(bpy)_3]I_2$. The shape of the two spectra is almost the same with hardly moving maxima position. The most striking difference between the spectra is the relative intensity of the maximun located around 420 nm: in the network, it is multiplied by a factor of 4 compared to the one observed at 300 nm. The comparison between the spectra of the network and of the precursor allows one to determine the absolute configuration of the hexacoordinated ruthenium(II) ion in the network following the principle that two related optically active tris(bischelated) ruthenium(II) ions have the same absolute configuration if they give a NCD signal of the same sign for a given transition.[62,63] The positive NCD signal at 300 nm is representative of a Λ configuration of the hexacoordinated Ru(II) ion.[64] It is present in both the precursor iodine salt and in the network so that the configuration of the template cation is preserved during the reaction. The similarity between the two spectra evidences that the main bands of the NCD spectra are essentially due to the template cation. They are actually attributed to intra-ligand or MLCT transitions of $[Ru(bpy)_3]^{2+}$.[64] The difference in intensity observed for the minimun at 420 nm for Λ-$[Ru(bpy)_3]^{2+}$ and at 429 nm for $\{\Lambda Cu_{1.28}\Lambda Ni_{0.72}\}_n$ can be attributed to the influence of the anionic network through weak intermolecular interactions on the electronic transition of the template cation. The weak dichroic signals of the metal ions of the μ-oxalato network cannot be observed, obscured by the intense bands of the template cation.

Table 7. Curie−Weiss Θ, Transition Temperature T_c, and Temperature T_c' of the Second Jump (When Present) of the Compounds $\{Cu_{2x}Ni_{2(1-x)}\}_n$

compound	Q/K	T_c/K	T_c'/K
$\{Cu_2\}_n$	−55	5	
$\{Cu_{1.8}Ni_{0.2}\}_n$	−91	7	
$\{Cu_{1.28}Ni_{0.72}\}_n$	−115	11	
$\{Cu_{0.88}Ni_{1.12}\}_n$	−125	28	12
$\{Cu_{0.3}Ni_{1.7}\}_n$	−149	28	14
$\{Ni_2\}_n$	−150	35	

The NCD curves thus establish that the arrangement of the bipyridine ligands around the ruthenium is preserved during the synthesis. But they do not provide a direct experimental conclusion about the configuration of the tris(bischelated) metal ions of the anionic network. Nevertheless, thanks to the diffraction patterns, the networks are known to be three-dimensional and to crystallize in the chiral space group $P4_132$. In such 3D compounds, the Δ (respectively Λ) enantiomer of the template cation can only lead to M-type (respectively P-type) anionic helices. In the helices, all the hexacoordinated metal ions adopt a homochiral arrangement of the metallic centers, that is, a Δ configuration for M and Λ for P.[15]

Magnetic Properties. The molar susceptibility χ_M is measured between 5 and 300 K all along the series. The χ_M vs T curves are below the one expected for isolated paramagnetic ions and in all the compounds except $\{Cu_2\}_n$; they present an abrupt increase at a critical temperature T_C. The $\chi_M T$ vs T curves show a smooth monotonic decrease when decreasing the temperature followed for all the compounds with $x \neq 1$ by an abrupt increase at low temperature at T_C (Figure 6a). $\chi_M T$ then reaches a maximun at 5 K for $\{Cu_{1.28}Ni_{0.72}\}_n$, 7 K for $\{Cu_{0.88}Ni_{1.12}\}_n$, 17 K for $\{Cu_{0.3}Ni_{1.7}\}_n$, and 20 K for $\{Ni_2\}_n$. In all cases, the χ_M^{-1} vs T curves are linear in the 100−300 K temperature range (Figure 6b). They can be fitted by a Curie−Weiss law $\chi_M^{-1} = (T - \Theta)/C$. The Weiss constants are negative and their absolute values increase when the copper-to-nickel ratio decreases (Table 7). Below 100 K, the experimental curve goes above the Curie−Weiss fit. Then at lower temperature, it slowly tends to zero (Figure 6b). These data are in agreement with a short-range antiferromag-

(62) Gillard, R. D. *Prog. Inorg. Chem.* **1966**, *7*, 215.
(63) Ziegler, M.; Von Zelewsky, A. *Coord. Chem. Rev.* **1998**, *177*, 257.
(64) McCaffery, A. J.; Mason, S. F.; Norman, B. J. *J. Chem. Soc. A* **1969**, 1428.

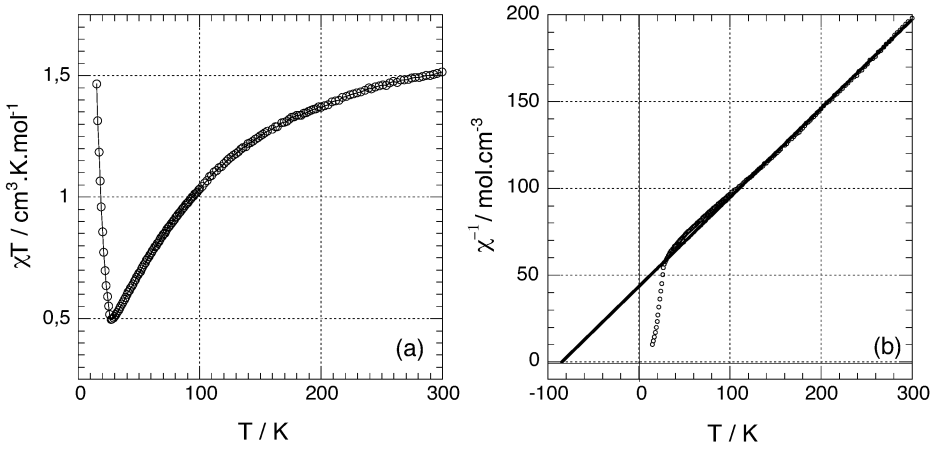

Figure 6. Thermal variation of χ^{-1} of $\{Cu_{1.28}Ni_{0.72}\}_n$: experimental (in an applied field of 0.1 T) (triangles) and Curie−Weiss fit of the high-temperature region (solid line).

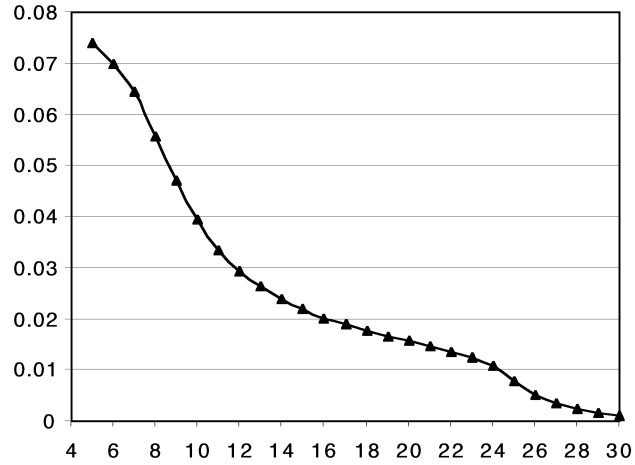

Figure 7. Field cooled magnetization of $\{Cu_{0.3}Ni_{1.7}\}_n$ in 0.01 T.

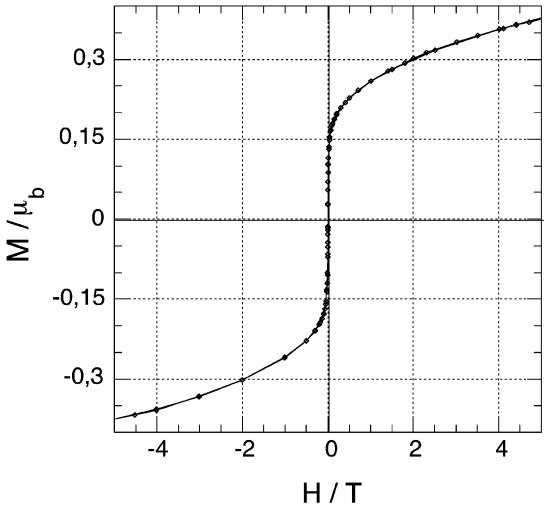

Figure 8. Hysteresis loop of $\{Cu_{1.28}Ni_{0.72}\}_n$ at 2 K.

netic interaction between the paramagnetic ions and with the appearance of some spontaneous magnetization at T_C.

The field cooled magnetization curves present one jump at T_C and a second jump for $0 < x \leq 0.25$ (Figure 7). T_C increases when x decreases. The first magnetization curves at 2 K present two parts: a fast increase at low field followed by a slow increase toward saturation, which cannot be reached in a 5 T field whatever the value of x (Figure 8). The hysteresis loops at 2 K show that the compounds are soft magnets with hardly measurable coercive forces.

The values of χ_M, the shape of the $\chi_M T$ vs T curves, and the sign of the Weiss constants Θ indicate the existence of a short-range antiferromagnetic interaction between the paramagnetic ions all along the series. The decrease of both Θ and T_cs indicates that the exchange interaction $|J|$ decreases when the copper contents increase. At first sight, this observation is surprising since oxalate-bridged copper binuclear complexes and chains are known to possess J value up to -380 cm^{-1} while Cu−Ni pairs exhibit J value of -52.7 cm^{-1} and Ni−Ni pairs exhibit J value of $-22-24$ cm^{-1}.[29,51,65] The interpretation of this evolution lies in the geometry around the copper(II) ion and in the overlap between neighboring magnetic orbitals. We examine successively the case of $\{Cu_2\}_n$, $\{Ni_2\}_n$, and then $\{Cu_{2x}Ni_{2(1-x)}\}_n$.

In μ-oxalato copper(II) chains or binuclear complexes, the unpaired electron of copper(II) is most often described by $d_{x^2-y^2}$ type singly occupied "magnetic" orbitals (Scheme 2). Three kinds of structures and overlaps are then possible: (a) Both magnetic orbitals lie in the plane of the oxalate and they overlap through both sides of the oxalate bridge (Scheme 2a). The overlap and the exchange ($J = -380$ cm^{-1}) are strong. (b) Both magnetic orbitals lie in a plane perpendicular to the oxalate and there is no more overlap through the oxalate (Scheme 2b). Overlap and exchange ($J = -13$ cm^{-1}) are weak. (c) One magnetic orbital is in the plane of the oxalate and the other one in a perpendicular plane (Scheme 2c). Only one carboxylate group of the oxalate ligand participates in the overlap. Overlap and exchange ($J = -75$ cm^{-1}) are intermediate.[58−60]

In light of the structural analysis—pointing out the presence of statistically distributed elongated octahedral copper(II)—it can be inferred that all the above interactions are present. The observed Θ value in $\{Cu_2\}_n$ (-55 K) corresponds mainly to case (c). In $\{Ni_2\}_n$, the Ni(II) environment is quasi-octahedral and two unpaired electrons are present in $d_{x^2-y^2}$ and d_{z^2} orbitals (magnetic

(65) Roman, P.; Guzman-Miralles, C.; Luque, A.; Beitia, J. I.; Cano, J.; Lloret, F.; Julve, M.; Alvarez, S. *Inorg. Chem.* **1996**, *35*, 3741.

Scheme 2

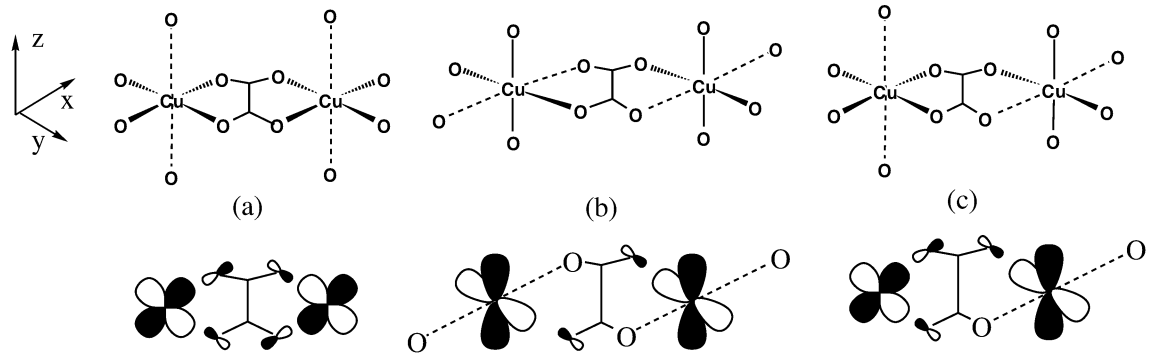

orbitals). The large Θ value observed (−150 K) can be safely assigned to the presence of the two antiferromagnetic exchange pathways $d_{x^2-y^2}-d_{x^2-y^2}$ (Scheme 2a) and $d_{z^2}-d_{z^2}$. The ferromagnetic exchange pathways $d_{x^2-y^2}-d_{z^2}$ (orthogonal orbitals) are much weaker. The large antiferromagnetic Ni−Ni interaction compared to the Cu−Cu one is obviously due to the systematic presence of the strong antiferromagnetic interaction $d_{x^2-y^2}-d_{x^2-y^2}$. In $\{Cu_{2x}Ni_{2(1-x)}\}_n$, due to the statistical distribution of copper(II) and nickel(II) ions on the same crystallographic site, a given metal ion presents a large variety of environments. The *J* values associated to nearest-neighbors interactions are thus widely distributed. The intermediate Θ values, which are related to the *J* values by a mean-field approach,[66] then correspond to a complex averaging of these *J* values.

The interpretation of the low-temperature magnetic behavior is less simple and deserves complementary work to fully understand the different features and check the following hypotheses: (i) ferrimagnetism and/or canted antiferromagnetism (weak ferromagnetism) to account for the abrupt increase of χ at T_C, the appearance of a nonzero magnetization at low temperature, and the fast increase of the initial magnetization at 2 K; (ii) the existence of two phases with different structures and transition temperatures and/or the presence of complex magnetic structures similar to the ones proposed by Yafet and Kittel[66] assuming non-negligible antiferromagnetic next-nearest-neighbor interaction between the metal atoms competing with the nearest-neighbors interaction, supported by the low values of T_c/Θ,[67] to account for the two jumps observed in the field-cooled magnetization for $0 < x < 0.25$.

To obtain a more precise view of theses complex magnetic behaviors, further investigations are planned, including the synthesis of new systems to evidence the next-nearest-neighbors interaction and neutron powder diffraction studies below the critical temperature.

Concluding Remarks

We have reported the synthesis and the optical and magnetic properties of 3D oxalate-based magnets including copper(II) and nickel(II) ions in the three-dimensional 10-gon 3-connected (10,3) anionic network. The synthesis of the networks fully exploits the templating activity of the resolved $[Ru(bpy)_3]^{2+}$ cation: through an enantioselective self-assembly, the cation imposes both its configuration and its symmetry to the anionic network though the metal ions used to build the μ-oxalato helices, nickel(II) and copper(II), do not usually adopt such a D_3 symmetry. The natural dichroism measurements confirm the validity of the synthetic approach to obtain resolved enantiomeric objects. The magnetic properties were revealed to be much richer than initially expected and further investigations are planned to reach a full understanding of the complex magnetic structure appearing at low temperature.

Acknowledgment. Authors thank for financial support CNRS (France), Université "Pierre et Marie Curie" (France), European community (TMR ERBFMBICT-972644 and FMRXCT980181), and European Science Foundation (Molecular Magnets Program).

Supporting Information Available: The data for the structure of the $\{Cu_2\}_n$ are deposited in the Cambridge DataBase with the number CCDC 191594. The complete set of magnetic data (χT and χ^{-1} vs *T* curves and hysteresis loop at 2 K) as well as the CIF for $\{Cu_2\}_n$ are available free of charge via the Internet at http://pubs.acs.org.

CM020330D

(66) Herpin, A. *Théorie du Magnétisme*; Presses Universitaires de France: Paris, 1968.
(67) Greedan, J. E. *J. Mater. Chem.* **2001**, *11*, 37.